Orosz, G., & Stepan, G. (2005). Subcritical Hopf bifurcations in a car-following model with reaction-time delay.

Subcritical Hopf bifurcations in a car-following model with reaction-time delay

By Gábor Orosz† and Gábor Stépán‡§

† *Bristol Centre for Applied Nonlinear Mathematics, Department of Engineering Mathematics, University of Bristol, Queen's Building, University Walk, Bristol BS8 1TR, United Kingdom,*
g.orosz@bristol.ac.uk

‡ *Department of Applied Mechanics, Budapest University of Technology and Economics, P.O. Box 91, Budapest H-1521, Hungary*
stepan@mm.bme.hu

§ *Research Group on Dynamics of Vehicles and Machines, Hungarian Academy of Sciences*

A nonlinear car-following model of highway traffic is considered, which includes the reaction-time delay of drivers. Linear stability analysis shows that the uniform flow equilibrium of the system loses its stability via Hopf bifurcations and thus oscillations can appear. The stability and amplitudes of the oscillations are determined with the help of normal-form calculations of the Hopf bifurcation that also handles the essential translational symmetry of the system. We show that the subcritical case of the Hopf bifurcation occurs robustly, which indicates the possibility of bistability. We also show how these oscillations lead to spatial wave formation as can be observed in real-world traffic flows.

Keywords: vehicular traffic, reaction-time delay, translational symmetry, subcritical Hopf bifurcation, bistability, stop-and-go waves

1. Introduction

The so-called *uniform flow equilibrium* of vehicles following each other on a road is a kind of steady state where equidistant vehicles travel with the same constant velocity. Ideally, this state is stable. Indeed, it is the goal of traffic management that drivers choose their traffic parameters to keep this state stable and also to reach their goal, that is, to travel with a speed close to their desired speed. Still, traffic jams often appear as congestion waves travelling opposite to the flow of vehicles (Kerner 1999). The formation of these traffic jams (waves) is often associated with the linear instability of the uniform flow equilibrium, which should be a rare occurrence. However, it is also well known among traffic engineers that certain events, such as a truck pulling out of its lane, may trigger traffic jams even when the uniform flow is stable. We investigate a delayed car-following model and provide a thorough examination of the subcriticality of Hopf bifurcations related to the drivers' reaction-time delay. This explains how a stable uniform flow can coexist with a stable traffic wave.

The car-following model analyzed in this paper was first introduced in (Bando *et al.* 1995) without the reaction-time delay of drivers, and that was investigated by numerical simulation. Then numerical continuation techniques were used in (Gasser *et al.* 2004; Berg & Wilson 2005) by applying the package AUTO (Doedel *et al.* 1997). Recently, Hopf calculations have been carried out in (Gasser *et al.* 2004) for arbitrary numbers of cars following each other on a ring.

The reaction-time delay of drivers was first introduced in (Bando *et al.* 1998), and its importance was then emphasized by the study (Davis 2003). In these papers numerical simulation was used to explore the nonlinear dynamics of the system. The first systematic global bifurcation analysis of the delayed model (Davis 2003) was presented in (Orosz *et al.* 2004*a*) where numerical continuation techniques, namely the package DDE-BIFTOOL (Engelborghs *et al.* 2001), were used. The continuation results were extended to large numbers of cars in (Orosz *et al.* 2004*b*) where the dynamics of oscillations, belonging to different traffic patterns, were analyzed as well. In this paper we perform an analytical Hopf bifurcation calculation and determine the criticality of the bifurcation as a function of parameters for arbitrary numbers of vehicles in the presence of the drivers' reaction delay.

While the models without delay are described by ordinary differential equations (ODEs), presenting the dynamics in finite-dimensional phase spaces, the appearance of the delay leads to delay differential equations (DDEs) and to infinite-dimensional phase spaces. The finite-dimensional bifurcation theory that is available in basic textbooks (Guckenheimer & Holmes 1997; Kuznetsov 1998) have been extended to DDEs in (Hale & Verduyn Lunel 1993; Diekmann *et al.* 1995; Kolmanovskii & Myshkis 1999; Hale *et al.* 2002). The infinite-dimensional dynamics make the bifurcation analysis more abstract. In particular, the Hopf normal form calculations require complicated algebraic formalism and algorithms, as is shown in (Hassard *et al.* 1981; Stépán 1986, 1989; Campbell & Bélair 1995; Stone & Campbell 2004; Orosz 2004). Recently, these Hopf calculations have been extended for systems with translational symmetry in (Orosz & Stépán 2004) which is an essential property of car-following models. This situation is similar to the S^1 symmetry that occurs in laser systems with delay, see (Verduyn Lunel & Krauskopf 2000; Rottschäfer & Krauskopf 2004). In (Orosz & Stépán 2004) the method was demonstrated on the over-simplified case of two cars on a ring. Here, these calculations are extended to arbitrarily many cars, providing general conclusions for the subcriticality of the bifurcations and its consequences for flow patterns. Our results are generalization of those in (Gasser *et al.* 2004) for the case without reaction-time delay. In particular, we prove that this delay makes the subcriticality of Hopf bifurcations robust.

2. Modelling Issues

The mathematical form of the car-following model in question was introduced and non-dimensionalized in (Orosz *et al.* 2004*a*). Here we recall the basic features of this model. Periodic boundary conditions are considered, i.e., n vehicles are distributed along a circular road of overall length L; see Fig. 1. (This could be interpreted as traffic on a circular road around a large city, e.g., the M25 around London, even though such roads usually possess higher complexity.) As the number of cars is increased the significance of the periodic boundary conditions usually tends to become smaller.

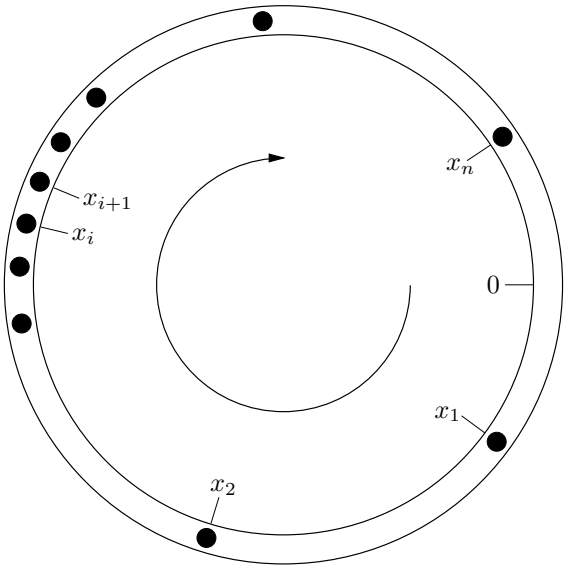

Figure 1. Vehicles flowing clockwise on circular road.

We assume that drivers have identical characteristics. Considering that the ith vehicle follows the $(i+1)$st vehicle and the nth car follows the 1st one, the equations of motion can be expressed as

$$\begin{aligned} \ddot{x}_i(t) &= \alpha\big(\mathrm{V}\left(x_{i+1}(t-1) - x_i(t-1)\right) - \dot{x}_i(t)\big), \quad i = 1, \ldots, n-1\,, \\ \ddot{x}_n(t) &= \alpha\big(\mathrm{V}\left(x_1(t-1) - x_n(t-1) + L\right) - \dot{x}_n(t)\big)\,, \end{aligned} \tag{2.1}$$

where dot stands for time derivative. The position, the velocity, and the acceleration of the ith car are denoted by x_i, $\dot{x}_i$, and $\ddot{x}_i$, respectively. The so-called *optimal velocity function* $\mathrm{V}\colon \mathbb{R}^+ \to \mathbb{R}^+$ depends on the distance of the cars $h_i = x_{i+1} - x_i$, which is usually called the *headway*. The argument of the headway contains the *reaction-time delay* of drivers which now is rescaled to 1. The parameter $\alpha > 0$ is known as the *sensitivity* and $1/\alpha > 0$ is often called the *relaxation time*. Due to the rescaling of the time with respect to the delay, the delay parameter is hidden in the sensitivity α and the magnitude of the function $\mathrm{V}(h)$; see details in (Orosz *et al.* 2004*a*).

Equation (2.1) expresses that each driver approaches an optimal velocity, given by $\mathrm{V}(h)$, with a characteristic relaxation time of $1/\alpha$, but reacts to its headway via a reaction-time delay 1. The general features of the optimal velocity function $\mathrm{V}(h)$ can be summarized as follows.

1. $\mathrm{V}(h)$ is continuous, nonnegative, and monotone increasing, since drivers want to travel faster as their headway increases. Note that in the vicinity of the Hopf bifurcation points, $\mathrm{V}(h)$ is required to be three times differentiable for the application of the Hopf Theorem (Guckenheimer & Holmes 1997; Kuznetsov 1998).

2. $\mathrm{V}(h) \to v^0$ as $h \to \infty$, where v^0 is known as the *desired speed*, which corresponds, for example, to the speed limit of the given highway. Drivers approach this speed with the relaxation time of $1/\alpha$ when the traffic is sparse.

3. $\mathrm{V}(h) \equiv 0$ for $h \in [0,1]$, where the so-called *jam headway* is the rescaled to 1, see (Orosz *et al.* 2004*a*). This means that drivers attempt to come to a full stop if their headways become less than the jam headway.

One might, for example, consider the optimal velocity function to take the form

$$\mathrm{V}(h) = \begin{cases} 0 & \text{if} \quad 0 \le h \le 1\,, \\ v^0 \dfrac{(h-1)^3}{1+(h-1)^3} & \text{if} \quad h > 1\,, \end{cases} \tag{2.2}$$

as already used in (Orosz *et al.* 2004*a*,*b*). This function is shown together with its derivatives in Fig. 2. Functions with shapes similar to (2.2) were used in (Bando *et al.* 1995, 1998; Davis 2003).

Note that the analytical calculations presented here are valid for *any* optimal velocity function $\mathrm{V}(h)$: it is not necessary to restrict ourself to a concrete function in contrast to the numerical simulations in (Bando *et al.* 1998; Davis 2003) and even to the numerical continuations in (Orosz *et al.* 2004*a*,*b*).

3. Translational Symmetry and Hopf Bifurcations

The stationary motion of the vehicles, the so-called *uniform flow equilibrium* is described by

$$x_i^{\mathrm{eq}}(t) = v^* t + x_i^*\,, \quad \Rightarrow \quad \dot{x}_i^{\mathrm{eq}}(t) \equiv v^*\,, \quad i = 1, \ldots, n\,, \tag{3.1}$$

where

$$x_{i+1}^* - x_i^* = x_1^* - x_n^* + L = L/n := h^*, \quad i = 1, \ldots, n-1\,, \tag{3.2}$$

and

$$v^* = \mathrm{V}(h^*) < v^0\,. \tag{3.3}$$

Note that one of the constants x_i^* can be chosen arbitrarily due to the translational symmetry along the ring. Henceforward, we consider the *average headway* $h^* = L/n$ as a bifurcation parameter. Increasing h^* increases the length L of the ring, which involves scaling all headways h_i accordingly.

Let us define the perturbation of the uniform flow equilibrium by

$$x_i^{\mathrm{p}}(t) \colon = x_i(t) - x_i^{\mathrm{eq}}(t)\,, \quad i = 1, \ldots, n\,. \tag{3.4}$$

Using Taylor series expansion of the optimal velocity function $\mathrm{V}(h)$ about $h = h^* (= L/n)$ up to third order of x_i^{p}, we can eliminate the zero-order terms

$$\begin{aligned} \ddot{x}_i^{\mathrm{p}}(t) &= -\alpha \dot{x}_i^{\mathrm{p}}(t) + \alpha \sum_{k=1}^{3} b_k(h^*) \big(x_{i+1}^{\mathrm{p}}(t-1) - x_i^{\mathrm{p}}(t-1)\big)^k\,, \quad i = 1, \ldots, n-1\,, \\ \ddot{x}_n^{\mathrm{p}}(t) &= -\alpha \dot{x}_n^{\mathrm{p}}(t) + \alpha \sum_{k=1}^{3} b_k(h^*) \big(x_1^{\mathrm{p}}(t-1) - x_n^{\mathrm{p}}(t-1)\big)^k\,, \end{aligned} \tag{3.5}$$

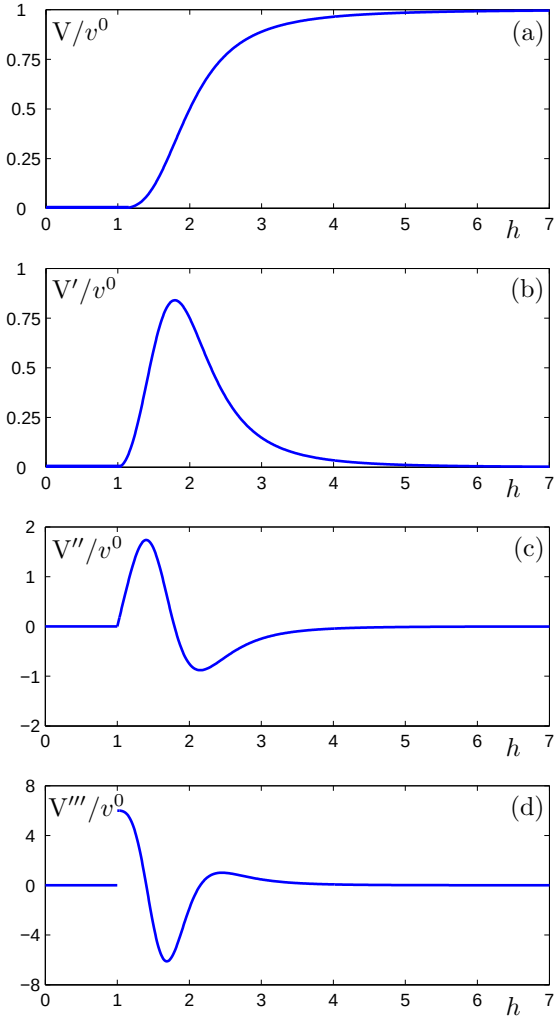

Figure 2. The optimal velocity function (2.2) is shown in panel (a), and its derivatives are displayed in panels (b)–(d).

where

$$b_1(h^*) = \mathrm{V}'(h^*)\,, \quad b_2(h^*) = \frac{1}{2}\mathrm{V}''(h^*)\,, \quad \text{and} \quad b_3(h^*) = \frac{1}{6}\mathrm{V}'''(h^*)\,. \tag{3.6}$$

At a critical/bifurcation point h^*_{cr} the derivatives take the values $b_{1\mathrm{cr}} = \mathrm{V}'(h^*_{\mathrm{cr}})$, $b_{2\mathrm{cr}} = \frac{1}{2}\mathrm{V}''(h^*_{\mathrm{cr}})$, and $b_{3\mathrm{cr}} = \frac{1}{6}\mathrm{V}'''(h^*_{\mathrm{cr}})$. Now and further on, prime denotes differentiation with respect to the headway.

Introducing the notation

$$y_i := \dot{x}^{\mathrm{p}}_i\,, \quad y_{i+n} := x^{\mathrm{p}}_i\,, \quad i = 1, \ldots, n\,, \tag{3.7}$$

equation (3.5) can be rewritten as

$$\dot{y}(t) = \tilde{\mathrm{L}}(h^*)y(t) + \tilde{\mathrm{R}}(h^*)y(t-1) + \tilde{F}\big(y(t-1);h^*\big)\,, \tag{3.8}$$

where $y\colon \mathbb{R} \to \mathbb{R}^{2n}$. The matrices $\tilde{\mathrm{L}}, \tilde{\mathrm{R}}\colon \mathbb{R} \to \mathbb{R}^{2n\times 2n}$ and the near-zero analytic function $\tilde{F}\colon \mathbb{R}^{2n}\times\mathbb{R}\to\mathbb{R}^{2n}$ are defined as

$$\begin{aligned} \tilde{\mathrm{L}}(h^*) &\equiv \begin{bmatrix} -\alpha \mathrm{I} & 0 \\ \mathrm{I} & 0 \end{bmatrix}\,, \qquad \tilde{\mathrm{R}}(h^*) = \begin{bmatrix} 0 & -\alpha b_1(h^*)\mathrm{A} \\ 0 & 0 \end{bmatrix}\,, \\ \tilde{F}\big(y(t-1);h^*\big) &= \begin{bmatrix} \alpha b_2(h^*) F_2\big(y(t-1)\big) + \alpha b_3(h^*) F_3\big(y(t-1)\big) \\ 0 \end{bmatrix}\,. \end{aligned} \tag{3.9}$$

Here $\mathrm{I} \in \mathbb{R}^{n\times n}$ stands for the n-dimensional identity matrix, while the matrix $\mathrm{A} \in \mathbb{R}^{n\times n}$ and the functions $F_2, F_3\colon \mathbb{R}^{2n}\to\mathbb{R}^n$ are defined as

$$\mathrm{A} = \begin{bmatrix} \ddots & \ddots & & \\ & 1 & -1 & \\ & & \ddots & \ddots \\ -1 & & & \ddots \end{bmatrix}\,, \quad F_k\big(y(t-1)\big) = \begin{bmatrix} \big(y_{n+2}(t-1) - y_{n+1}(t-1)\big)^k \\ \big(y_{n+3}(t-1) - y_{n+2}(t-1)\big)^k \\ \vdots \\ \big(y_{n+1}(t-1) - y_{2n}(t-1)\big)^k \end{bmatrix}\,, \quad k = 2,3\,. \tag{3.10}$$

System (3.8) possesses a translational symmetry, therefore the matrices $\tilde{\mathrm{L}}(h^*), \tilde{\mathrm{R}}(h^*)$ satisfy

$$\det\big(\tilde{\mathrm{L}}(h^*) + \tilde{\mathrm{R}}(h^*)\big) = 0\,, \tag{3.11}$$

that is, the Jacobian $\big(\tilde{\mathrm{L}}(h^*) + \tilde{\mathrm{R}}(h^*)\big)$ has a zero eigenvalue

$$\lambda_0(h^*) = 0\,, \tag{3.12}$$

for any value of parameter h^*. Furthermore, the near-zero analytic function $\tilde{F}$ preserves this translational symmetry, that is,

$$\tilde{F}\big(y(t-1)+c;h^*\big) = \tilde{F}\big(y(t-1);h^*\big)\,, \tag{3.13}$$

for all $c \neq 0$ satisfying $\big(\tilde{\mathrm{L}}(h^*) + \tilde{\mathrm{R}}(h^*)\big)c = 0$; see details in (Orosz & Stépán 2004).

The steady state $y(t) \equiv 0$ of (3.8) corresponds to the uniform flow equilibrium (3.1) of the original system (2.1). Considering the linear part of (3.8) and using the trial solution $y(t) = C\mathrm{e}^{\lambda t}$ with $C \in \mathbb{C}^{2n}$ and $\lambda \in \mathbb{C}$, the characteristic equation becomes

$$D\big(\lambda, b_1(h^*)\big) = \big(\lambda^2 + \alpha\lambda + \alpha b_1(h^*)\,\mathrm{e}^{-\lambda}\big)^n - \big(\alpha b_1(h^*)\,\mathrm{e}^{-\lambda}\big)^n = 0\,. \tag{3.14}$$

According to (3.11), the relevant zero eigenvalue (3.12) is one of the infinitely many characteristic exponents that satisfy (3.14). This exponent exists for any value of the parameter b_1, that is, for any value of the bifurcation parameter h^*.

At a bifurcation point defined by $b_1 = b_{1\mathrm{cr}}$, i.e., by $h^* = h^*_{\mathrm{cr}}$, Hopf bifurcations may occur in the complementary part of the phase space spanned by the eigenspace of the zero exponent (3.12). Then there exists a complex conjugate pair of pure imaginary characteristic exponents

$$\lambda_{1,2}(h^*_{\mathrm{cr}}) = \pm \mathrm{i}\omega\,, \quad \omega \in \mathbb{R}^+\,, \tag{3.15}$$

which satisfies (3.14). To find the Hopf boundaries in the parameter space we substitute $\lambda_1 = \mathrm{i}\omega$ into (3.14). Separation of the real and imaginary parts gives

$$\begin{aligned} b_{1\mathrm{cr}} &= \frac{\omega}{2\cos(\omega - \frac{k\pi}{n})\sin(\frac{k\pi}{n})}\,, \\ \alpha &= -\omega\cot(\omega - \tfrac{k\pi}{n})\,. \end{aligned} \tag{3.16}$$

The so-called wave number k can take the values $k = 1, \ldots, n/2$ (for even n) and $k = 1, \ldots (n-1)/2$ (for odd n). The wave numbers $k > n/2$ are not considered since they belong to conjugated waves producing the same spatial pattern. Note that $k = 1$ belongs to the stability boundary of the uniform flow equilibrium, while the cases $k > 1$ result in further oscillation modes around the already unstable equilibrium. Furthermore, for each k the resulting frequency is bounded so that $\omega \in (0, \frac{k\pi}{n})$; see (Orosz *et al.* 2004*a*,*b*).

Note also that the function $b_1(h^*) = \mathrm{V}'(h^*)$ shown in Fig. 2(b) is non-monotonous, and so a $b_{1\mathrm{cr}}$ boundary typically leads either to two or to zero h^*_{cr} boundaries. For a fixed wave number k these boundaries tend to finite values of h^* as $n \to \infty$, as is shown in (Orosz *et al.* 2004*b*). Using trigonometric identities, (3.16) can be transformed to

$$\begin{aligned} \cos\omega &= \frac{\omega}{2b_{1\mathrm{cr}}}\left(\frac{\omega}{\alpha} + \cot(\tfrac{k\pi}{n})\right)\,, \\ \sin\omega &= \frac{\omega}{2b_{1\mathrm{cr}}}\left(1 - \frac{\omega}{\alpha}\cot(\tfrac{k\pi}{n})\right)\,, \end{aligned} \tag{3.17}$$

which is a useful form used later in the Hopf calculation together with the resulting form

$$\frac{4b_{1\mathrm{cr}}^2}{\omega^2}\sin^2(\tfrac{k\pi}{n}) = 1 + \frac{\omega^2}{\alpha^2}\,. \tag{3.18}$$

With the help of the identity

$$\frac{\left(1 + \mathrm{i}\cot(\frac{k\pi}{n})\right)^{n-1}}{\left(1 - \mathrm{i}\cot(\frac{k\pi}{n})\right)^{n-1}} = \frac{1 - \mathrm{i}\cot(\frac{k\pi}{n})}{1 + \mathrm{i}\cot(\frac{k\pi}{n})}\,, \tag{3.19}$$

we can calculate the following necessary condition for Hopf bifurcation as the parameter b_1 is varied as

$$\mathrm{Re}\left(\frac{\mathrm{d}\lambda_1(b_{1\mathrm{cr}})}{\mathrm{d}b_1}\right) = \mathcal{E}\frac{1}{b_{1\mathrm{cr}}}\left(\omega^2 + \alpha^2 + \alpha\right) > 0\,, \tag{3.20}$$

where

$$\mathcal{E} = \left(\left(\tfrac{\alpha}{\omega} - \omega\right)^2 + \left(2 + \alpha\right)^2\right)^{-1}\,. \tag{3.21}$$

Since (3.20) is always positive this Hopf condition is always satisfied. Now, using the chain rule and definition (3.6), condition (3.20) can be calculated further as the average headway h^* is varied to give

$$\mathrm{Re}\left(\lambda_1'(h^*_{\mathrm{cr}})\right) = \mathrm{Re}\left(\frac{\mathrm{d}\lambda_1(b_{1\mathrm{cr}})}{\mathrm{d}b_1}\,b_1'(h^*_{\mathrm{cr}})\right) = \mathcal{E}\frac{2b_{2\mathrm{cr}}}{b_{1\mathrm{cr}}}\left(\omega^2 + \alpha^2 + \alpha\right) \neq 0\,. \tag{3.22}$$

This condition is fulfilled if and only if $b_{2\mathrm{cr}} \neq 0$, which is usually satisfied except at some special points. For example, the function $\mathrm{V}''(h)$ shown in Fig. 2(c) becomes zero at a single point over the interval $h \in (1, \infty)$. Notice that $\mathrm{V}''(h)$ is zero for $h \in [0, 1]$ and for $h \to \infty$, but the critical headway h_{cr} never takes these values for $\alpha > 0$.

4. Operator Differential Equations and Related Eigenvectors

The delay-differential equation (3.8) can be rewritten in the form of an operator-differential equation (OpDE). For the critical bifurcation parameter h^*_{cr}, we obtain

$$\dot{y}_t = \mathcal{A} y_t + \mathcal{F}(y_t)\,, \tag{4.1}$$

where the dot still refers to differentiation with respect to the time t and $y_t \colon \mathbb{R} \to \mathbb{X}_{\mathbb{R}^{2n}}$ is defined by the shift $y_t(\vartheta) = y(t+\vartheta)$, $\vartheta \in [-1, 0]$ on the function space $\mathbb{X}_{\mathbb{R}^{2n}}$ of continuous functions mapping $[-1, 0] \to \mathbb{R}^{2n}$. The linear and nonlinear operators $\mathcal{A}$, $\mathcal{F} \colon \mathbb{X}_{\mathbb{R}^{2n}} \to \mathbb{X}_{\mathbb{R}^{2n}}$ are defined as

$$\mathcal{A}\phi(\vartheta) = \begin{cases} \dfrac{\partial}{\partial \vartheta}\phi(\vartheta)\,, & \text{if} \quad -1 \leq \vartheta < 0\,, \\ \mathrm{L}\phi(0) + \mathrm{R}\phi(-1)\,, & \text{if} \quad \vartheta = 0\,, \end{cases} \tag{4.2}$$

$$\mathcal{F}(\phi)(\vartheta) = \begin{cases} 0\,, & \text{if} \quad -1 \leq \vartheta < 0\,, \\ F(\phi(-1))\,, & \text{if} \quad \vartheta = 0\,, \end{cases} \tag{4.3}$$

where the matrices $\mathrm{L}, \mathrm{R} \in \mathbb{R}^{2n \times 2n}$, and the nonlinear function $F \colon \mathbb{R}^{2n} \to \mathbb{R}^{2n}$ are given by

$$\mathrm{L} = \tilde{\mathrm{L}}(h^*_{\mathrm{cr}})\,, \quad \mathrm{R} = \tilde{\mathrm{R}}(h^*_{\mathrm{cr}})\,, \quad \text{and} \quad F\big(y(t-1)\big) = \tilde{F}\big(y(t-1); h^*_{\mathrm{cr}}\big)\,. \tag{4.4}$$

The translational symmetry conditions (3.11) and (3.13) are inherited, that is,

$$\det(\mathrm{L} + \mathrm{R}) = 0\,, \tag{4.5}$$

and

$$\mathcal{F}(y_t + c) = \mathcal{F}(y_t) \quad \Leftrightarrow \quad F\big(y(t-1) + c\big) = F\big(y(t-1)\big)\,, \tag{4.6}$$

for all $c \neq 0$ satisfying $(\mathrm{L} + \mathrm{R})c = 0$.

In order to avoid singularities in Hopf calculations we follow the methodology and algorithm of (Orosz & Stépán 2004) and eliminate the eigendirection belonging to the relevant zero eigenvalue $\lambda_0 = 0$ (3.12). The corresponding eigenvector $s_0 \in \mathbb{X}_{\mathbb{R}^{2n}}$ satisfies

$$\mathcal{A} s_0 = \lambda_0 s_0 \quad \Rightarrow \quad \mathcal{A} s_0 = 0\,, \tag{4.7}$$

which, applying the definition (4.2) of operator $\mathcal{A}$, leads to a boundary value problem with the constant solution

$$s_0(\vartheta) \equiv S_0 \in \mathbb{R}^{2n}\,, \quad \text{satisfying} \quad (\mathrm{L} + \mathrm{R}) S_0 = 0\,. \tag{4.8}$$

One finds that

$$S_0 = p \begin{bmatrix} 0 \\ E \end{bmatrix}\,, \tag{4.9}$$

where each component of the vector $E \in \mathbb{R}^n$ is equal to 1. Here $p \in \mathbb{R}$ is a scalar that can be chosen freely, in particular, we choose $p = 1$.

In order to project the system to s_0 and to its complementary space, we also need the adjoint operator

$$\mathcal{A}^*\psi(\sigma) = \begin{cases} -\dfrac{\partial}{\partial\sigma}\psi(\sigma)\,, & \text{if} \quad 0 \le \sigma < 1\,, \\ \mathrm{L}^*\psi(0) + \mathrm{R}^*\psi(1)\,, & \text{if} \quad \sigma = 0\,, \end{cases} \tag{4.10}$$

where * denotes either adjoint operator or transposed conjugate vector and matrix. The eigenvector $n_0 \in \mathbb{X}^*_{\mathbb{R}^{2n}}$ of $\mathcal{A}^*$ associated with the eigenvalue $\lambda_0^* = 0$ satisfies

$$\mathcal{A}^* n_0 = \lambda_0^* n_0 \quad \Rightarrow \quad \mathcal{A}^* n_0 = 0\,. \tag{4.11}$$

This gives another boundary value problem which has the constant solution

$$n_0(\vartheta) \equiv N_0 \in \mathbb{R}^{2n}\,, \quad \text{satisfying} \quad (\mathrm{L}^* + \mathrm{R}^*)N_0 = 0\,. \tag{4.12}$$

Here we obtain

$$N_0 = \hat{p} \begin{bmatrix} E \\ \alpha E \end{bmatrix}\,. \tag{4.13}$$

However, $\hat{p} \in \mathbb{R}$ is not free, but is determined by the normality condition

$$\langle n_0, s_0 \rangle = 1\,. \tag{4.14}$$

Defining the inner product

$$\langle \psi, \phi \rangle = \psi^*(0)\phi(0) + \int_{-1}^{0} \psi^*(\xi + 1)\mathrm{R}\phi(\xi)\mathrm{d}\xi\,, \tag{4.15}$$

condition (4.14) gives the scalar equation

$$N_0^*(\mathrm{I} + \mathrm{R})S_0 = 1\,, \tag{4.16}$$

from which we obtain

$$\hat{p} = \frac{1}{n\alpha}\,. \tag{4.17}$$

Note that, as the vectors s_0 and n_0 are the right and left eigenvectors of the operator $\mathcal{A}$ belonging to the eigenvalues $\lambda_0 = 0$ and $\lambda_0^* = 0$, similarly the vectors S_0 and N_0 are the right and left eigenvectors of the matrix $(\mathrm{L} + \mathrm{R})$, belonging to the same eigenvalues.

With the help of the eigenvectors s_0 and n_0, the new state variables $z_0 \colon \mathbb{R} \to \mathbb{R}$ and $y_t^- \colon \mathbb{R} \to \mathbb{X}_{\mathbb{R}^{2n}}$ are defined as

$$\begin{cases} z_0 = \langle n_0, y_t \rangle\,, \\ y_t^- = y_t - z_0 s_0\,. \end{cases} \tag{4.18}$$

Using the derivation given in (Orosz & Stépán 2004) we split the OpDE (4.1) into

$$\begin{aligned} \dot{z}_0 &= N_0^* \mathcal{F}(y_t^-)(0)\,, \\ \dot{y}_t^- &= \mathcal{A} y_t^- + \mathcal{F}(y_t^-) - N_0^* \mathcal{F}(y_t^-)(0) S_0\,. \end{aligned} \tag{4.19}$$

Its second part is already fully decoupled, and can be redefined as

$$\dot{y}_t^- = \mathcal{A} y_t^- + \mathcal{F}^-(y_t^-)\,, \tag{4.20}$$

where the new nonlinear operator $\mathcal{F}^-\colon \mathbb{X}_{\mathbb{R}^{2n}} \to \mathbb{X}_{\mathbb{R}^{2n}}$ assumes the form

$$\mathcal{F}^-(\phi)(\vartheta) = \begin{cases} -N_0^* \mathcal{F}(\phi)(0) S_0\,, & \text{if} \quad -1 \le \vartheta < 0\,, \\ \mathcal{F}(\phi)(0) - N_0^* \mathcal{F}(\phi)(0) S_0\,, & \text{if} \quad \vartheta = 0\,. \end{cases} \tag{4.21}$$

Considering $\mathcal{F}(\phi)(0) = F(\phi(-1))$ given by (4.3), and using the expressions (3.9,3.10,4.4), and the eigenvectors (4.9,4.13), we obtain

$$\begin{aligned} N_0^* \mathcal{F}(y_t^-)(0) S_0 &= N_0^* F\big(y(t-1)\big) S_0 \\ &= \frac{1}{n} \sum_{k=2,3} \left(b_{k\mathrm{cr}} \sum_{i=1}^{n} \big(y_{n+i+1}(t-1) - y_{n+i}(t-1)\big)^k \right) \begin{bmatrix} 0 \\ E \end{bmatrix}\,, \end{aligned} \tag{4.22}$$

where the definition $y_{2n+1} := y_{n+1}$ is applied. Note that the system reduction related to the translational symmetry changes the nonlinear operator of the system while the linear operator remains the same. This change has an essential role in the center-manifold reduction presented below.

Let us consider a Hopf bifurcation at a critical point h_{cr}^*. First, we determine the real and imaginary parts $s_1, s_2 \in \mathbb{X}_{\mathbb{R}^{2n}}$ of the eigenvector of the linear operator $\mathcal{A}$, which belongs to the critical eigenvalue $\lambda_1 = \mathrm{i}\omega$ (3.15), that is,

$$\mathcal{A} s_1(\vartheta) = -\omega s_2(\vartheta)\,, \quad \mathcal{A} s_2(\vartheta) = \omega s_1(\vartheta)\,. \tag{4.23}$$

After the substitution of definition (4.2) of $\mathcal{A}$, the solution of the resulting boundary value problem can be written as

$$\begin{bmatrix} s_1(\vartheta) \\ s_2(\vartheta) \end{bmatrix} = \begin{bmatrix} S_1 \\ S_2 \end{bmatrix} \cos(\omega\vartheta) + \begin{bmatrix} -S_2 \\ S_1 \end{bmatrix} \sin(\omega\vartheta)\,, \tag{4.24}$$

with constant vectors $S_1, S_2 \in \mathbb{R}^{2n}$ satisfying the homogeneous equation

$$\begin{bmatrix} \mathrm{L} + \mathrm{R}\cos\omega & \omega\mathrm{I} + \mathrm{R}\sin\omega \\ -(\omega\mathrm{I} + \mathrm{R}\sin\omega) & \mathrm{L} + \mathrm{R}\cos\omega \end{bmatrix} \begin{bmatrix} S_1 \\ S_2 \end{bmatrix} = \begin{bmatrix} 0 \\ 0 \end{bmatrix}\,. \tag{4.25}$$

Using formula (3.17) for the Hopf boundary, the above $4n$-dimensional equation leads to

$$\left.\begin{aligned} S_{2,i} &= \omega S_{1,n+i} \\ S_{2,n+i} &= -\frac{1}{\omega} S_{1,i} \end{aligned}\right\} \quad \text{for} \quad i = 1, \dots, n\,, \tag{4.26}$$

and to the $2n$-dimensional equation

$$\begin{bmatrix} -\frac{1}{\omega}\cot(\frac{k\pi}{n})\mathrm{A} & \mathrm{B} \\ \mathrm{B} & \frac{1}{\omega}\cot(\frac{k\pi}{n})\mathrm{A} \end{bmatrix} S_1 = 0\,, \tag{4.27}$$

where $\mathrm{A} \in \mathbb{R}^{n\times n}$ is defined by (3.10) and $\mathrm{B} \in \mathbb{R}^{n\times n}$ is given by

$$\mathrm{B} = \begin{bmatrix} \ddots & \ddots & & \\ & 1 & 1 & \\ & & \ddots & \ddots \\ 1 & & & \ddots \end{bmatrix}\,. \tag{4.28}$$

Solving (4.27) one may obtain

$$S_1 = u \begin{bmatrix} C \\ \frac{1}{\omega} S \end{bmatrix} + v \begin{bmatrix} S \\ -\frac{1}{\omega} C \end{bmatrix}, \quad S_2 = u \begin{bmatrix} S \\ -\frac{1}{\omega} C \end{bmatrix} - v \begin{bmatrix} C \\ \frac{1}{\omega} S \end{bmatrix}, \tag{4.29}$$

where the scalar parameters u and v can be chosen arbitrarily and the vectors $C, S \in \mathbb{R}^n$ are

$$C = \begin{bmatrix} \cos(\frac{2k\pi}{n} 1) \\ \cos(\frac{2k\pi}{n} 2) \\ \vdots \\ \cos(\frac{2k\pi}{n} n) \end{bmatrix}, \quad S = \begin{bmatrix} \sin(\frac{2k\pi}{n} 1) \\ \sin(\frac{2k\pi}{n} 2) \\ \vdots \\ \sin(\frac{2k\pi}{n} n) \end{bmatrix}, \tag{4.30}$$

with the wave number k used in (3.16,3.17). The cyclic permutation of the components in C and S results in further vectors S_1, S_2 that still satisfy (4.25). This result corresponds to the $\mathbb{Z}^n$ symmetry of the system, that is, all the cars have the same dynamic characteristics. Choosing $u = 1$ and $v = 0$ yields

$$S_1 = \begin{bmatrix} C \\ \frac{1}{\omega} S \end{bmatrix}, \quad S_2 = \begin{bmatrix} S \\ -\frac{1}{\omega} C \end{bmatrix}. \tag{4.31}$$

The real and imaginary parts $n_1, n_2 \in \mathbb{X}^*_{\mathbb{R}^{2n}}$ of the eigenvector of the adjoint operator $\mathcal{A}^*$ associated with $\lambda_1^* = -\mathrm{i}\omega$ are determined by

$$\mathcal{A}^* n_1(\sigma) = \omega n_2(\sigma), \quad \mathcal{A}^* n_2(\sigma) = -\omega n_1(\sigma). \tag{4.32}$$

The use of definition (4.10) of $\mathcal{A}^*$ leads to another boundary value problem having the solution

$$\begin{bmatrix} n_1(\sigma) \\ n_2(\sigma) \end{bmatrix} = \begin{bmatrix} N_1 \\ N_2 \end{bmatrix} \cos(\omega\sigma) + \begin{bmatrix} -N_2 \\ N_1 \end{bmatrix} \sin(\omega\sigma), \tag{4.33}$$

where the constant vectors $N_1, N_2 \in \mathbb{R}^{2n}$ satisfy

$$\begin{bmatrix} \mathrm{L}^* + \mathrm{R}^* \cos\omega & -(\omega \mathrm{I} + \mathrm{R}^* \sin\omega) \\ \omega \mathrm{I} + \mathrm{R}^* \sin\omega & \mathrm{L}^* + \mathrm{R}^* \cos\omega \end{bmatrix} \begin{bmatrix} N_1 \\ N_2 \end{bmatrix} = \begin{bmatrix} 0 \\ 0 \end{bmatrix}. \tag{4.34}$$

The application of (3.17) simplifies this $4n$-dimensional equation to

$$\left.\begin{aligned} N_{1,n+i} &= \alpha N_{1,i} + \omega N_{2,i} \\ N_{2,n+i} &= -\omega N_{1,i} + \alpha N_{2,i} \end{aligned}\right\} \quad \text{for} \quad i = 1, \ldots, n, \tag{4.35}$$

and to the $2n$-dimensional equation

$$\begin{bmatrix} -\cot(\frac{k\pi}{n})\mathrm{A} & \mathrm{B} \\ \mathrm{B} & \cot(\frac{k\pi}{n})\mathrm{A} \end{bmatrix} N_\cup = 0, \tag{4.36}$$

where $N_\cup \in \mathbb{R}^{2n}$ is defined as

$$\left.\begin{aligned} N_{\cup,i} &= N_{1,i} \\ N_{\cup,n+i} &= N_{2,i} \end{aligned}\right\} \quad \text{for} \quad i = 1, \ldots, n. \tag{4.37}$$

The solution of (4.36) can be written as

$$N_{\cup} = \hat{u} \begin{bmatrix} C \\ S \end{bmatrix} + \hat{v} \begin{bmatrix} S \\ -C \end{bmatrix} , \tag{4.38}$$

which results in

$$N_1 = \hat{u} \begin{bmatrix} C \\ \alpha C + \omega S \end{bmatrix} + \hat{v} \begin{bmatrix} S \\ \alpha S - \omega C \end{bmatrix} , \quad N_2 = \hat{u} \begin{bmatrix} S \\ \alpha S - \omega C \end{bmatrix} - \hat{v} \begin{bmatrix} C \\ \alpha C + \omega S \end{bmatrix} . \tag{4.39}$$

The scalar parameters $\hat{u}, \hat{v}$ are determined by the orthonormality conditions

$$\langle n_1, s_1 \rangle = 1 , \quad \langle n_1, s_2 \rangle = 0 , \tag{4.40}$$

which, using the inner product definition (4.15), results in the two scalar equations

$$\frac{1}{2} \begin{bmatrix} S_1^* \left(2\mathrm{I} + \mathrm{R}^* \left(\cos\omega + \frac{\sin\omega}{\omega}\right)\right) + S_2^* \mathrm{R}^* \sin\omega & -S_1^* \mathrm{R}^* \sin\omega + S_2^* \mathrm{R}^* \left(\cos\omega - \frac{\sin\omega}{\omega}\right) \\ -S_1^* \mathrm{R}^* \sin\omega + S_2^* \left(2\mathrm{I} + \mathrm{R}^* \left(\cos\omega + \frac{\sin\omega}{\omega}\right)\right) & -S_1^* \mathrm{R}^* \left(\cos\omega - \frac{\sin\omega}{\omega}\right) - S_2^* \mathrm{R}^* \sin\omega \end{bmatrix} \times \\ \times \begin{bmatrix} N_1 \\ N_2 \end{bmatrix} = \begin{bmatrix} 1 \\ 0 \end{bmatrix} . \tag{4.41}$$

Substituting (3.17,4.31,4.39) into (4.41) and using the second order trigonometric identities (A 4–A 6), we obtain

$$\frac{n}{2} \begin{bmatrix} 2+\alpha & \frac{\alpha}{\omega} - \omega \\ -\left(\frac{\alpha}{\omega} - \omega\right) & 2+\alpha \end{bmatrix} \begin{bmatrix} \hat{u} \\ \hat{v} \end{bmatrix} = \begin{bmatrix} 1 \\ 0 \end{bmatrix} , \tag{4.42}$$

with the solution

$$\begin{bmatrix} \hat{u} \\ \hat{v} \end{bmatrix} = \mathcal{E} \frac{2}{n} \begin{bmatrix} 2+\alpha \\ \frac{\alpha}{\omega} - \omega \end{bmatrix} , \tag{4.43}$$

where $\mathcal{E}$ is defined by (3.21). The substitution of (4.43) into (4.39) leads to

$$\begin{aligned} N_1 &= \mathcal{E} \frac{2}{n} \begin{bmatrix} (2+\alpha)C + \left(\frac{\alpha}{\omega} - \omega\right) S \\ (\alpha^2 + \alpha + \omega^2) C + \left(\frac{\alpha^2}{\omega} + 2\,\omega\right) S \end{bmatrix} , \\ N_2 &= \mathcal{E} \frac{2}{n} \begin{bmatrix} (2+\alpha)S - \left(\frac{\alpha}{\omega} - \omega\right) C \\ (\alpha^2 + \alpha + \omega^2) S - \left(\frac{\alpha^2}{\omega} + 2\,\omega\right) C \end{bmatrix} . \end{aligned} \tag{4.44}$$

As $s_1 + \mathrm{i}s_2$ and $n_1 + \mathrm{i}n_2$ are the right and left eigenvectors of the operator $\mathcal{A}$ belonging to the eigenvalues $\lambda_1 = \mathrm{i}\omega$ and $\lambda_1^* = -\mathrm{i}\omega$, the vectors $S_1 + \mathrm{i}S_2$ and $N_1 + \mathrm{i}N_2$ are similarly the right and left eigenvectors of the matrix (L+R) belonging to the same eigenvalues.

5. Center-manifold Reduction

With the help of the eigenvectors s_1, s_2 and n_1, n_2, we introduce the new state variables

$$\begin{cases} z_1 = \langle n_1, y_t^- \rangle , \\ z_2 = \langle n_2, y_t^- \rangle , \\ w = y_t^- - z_1 s_1 - z_2 s_2 , \end{cases} \tag{5.1}$$

where $z_1, z_2 \colon \mathbb{R} \to \mathbb{R}$ and $w \colon \mathbb{R} \to \mathbb{X}_{\mathbb{R}^{2n}}$. Using the derivation presented in (Orosz & Stépán 2004) we can reduce OpDE (4.20) to the form

$$\begin{bmatrix} \dot{z}_1 \\ \dot{z}_2 \\ \dot{w} \end{bmatrix} = \begin{bmatrix} 0 & \omega & \mathcal{O} \\ -\omega & 0 & \mathcal{O} \\ 0 & 0 & \mathcal{A} \end{bmatrix} \begin{bmatrix} z_1 \\ z_2 \\ w \end{bmatrix} + \begin{bmatrix} (N_1^* - q_1 N_0^*)\mathcal{F}(z_1 s_1 + z_2 s_2 + w)(0) \\ (N_2^* - q_2 N_0^*)\mathcal{F}(z_1 s_1 + z_2 s_2 + w)(0) \\ -\sum_{j=1,2}(N_j^* - q_j N_0^*)\mathcal{F}(z_1 s_1 + z_2 s_2 + w)(0) s_j + \mathcal{F}^-(z_1 s_1 + z_2 s_2 + w) \end{bmatrix}. \tag{5.2}$$

The scalar parameters q_1, q_2 are induced by the translational symmetry and their expressions are determined in (Orosz & Stépán 2004) as

$$\begin{aligned} q_1 &= \left(N_1^*(\mathrm{I} + \tfrac{\sin\omega}{\omega}\mathrm{R}) - N_2^* \tfrac{1-\cos\omega}{\omega}\mathrm{R}\right) S_0\,, \\ q_2 &= \left(N_1^* \tfrac{1-\cos\omega}{\omega}\mathrm{R} + N_2^*(\mathrm{I} + \tfrac{\sin\omega}{\omega}\mathrm{R})\right) S_0\,. \end{aligned} \tag{5.3}$$

Since in our case $\mathrm{R}S_0 = N_1^* S_0 = N_2^* S_0 = 0$, we obtain

$$q_1 = q_2 = 0\,. \tag{5.4}$$

The power series form of (5.2) is also given in (Orosz & Stépán 2004) as

$$\begin{bmatrix} \dot{z}_1 \\ \dot{z}_2 \\ \dot{w} \end{bmatrix} = \begin{bmatrix} 0 & \omega & \mathcal{O} \\ -\omega & 0 & \mathcal{O} \\ 0 & 0 & \mathcal{A} \end{bmatrix} \begin{bmatrix} z_1 \\ z_2 \\ w \end{bmatrix} + \begin{bmatrix} \sum_{j,k\geq 0}^{j+k=2,3} f_{jk}^{(1)} z_1^j z_2^k \\ \sum_{j,k\geq 0}^{j+k=2,3} f_{jk}^{(2)} z_1^j z_2^k \\ \frac{1}{2}\sum_{j,k\geq 0}^{j+k=2}\left(F_{jk}^{(3\mathrm{c})}\cos(\omega\vartheta) + F_{jk}^{(3\mathrm{s})}\sin(\omega\vartheta)\right) z_1^j z_2^k \end{bmatrix}$$

$$+ \begin{bmatrix} F_{10}^{(1)*}\mathrm{R}w(-1)z_1 + F_{01}^{(1)*}\mathrm{R}w(-1)z_2 \\ F_{10}^{(2)*}\mathrm{R}w(-1)z_1 + F_{01}^{(2)*}\mathrm{R}w(-1)z_2 \\ \frac{1}{2}\begin{cases} \sum_{j,k\geq 0}^{j+k=2} F_{jk}^{(3-)} z_1^j z_2^k\,, & \text{if} \quad -1 \leq \vartheta < 0\,, \\ \sum_{j,k\geq 0}^{j+k=2}\left(F_{jk}^{(3)} + F_{jk}^{(3-)}\right) z_1^j z_2^k\,, & \text{if} \quad \vartheta = 0 \end{cases} \end{bmatrix}, \tag{5.5}$$

where the subscripts of the constant coefficients $f_{jk}^{(1,2)} \in \mathbb{R}$ and the vector ones $F_{jk}^{(1,2,3)} \in \mathbb{R}^{2n}$ refer to the corresponding jth and kth orders of z_1 and z_2, respectively. The terms with the coefficients $F_{jk}^{(3\mathrm{s})}$, $F_{jk}^{(3\mathrm{c})}$ come from the linear combinations of $s_1(\vartheta)$ and $s_2(\vartheta)$. The translational symmetry only enters through the terms with coefficients $F_{jk}^{(3-)}$, so that the terms with coefficients $F_{jk}^{(3)}$ and $F_{jk}^{(3-)}$ refer to the structure of the modified nonlinear operator $\mathcal{F}^-$ (4.21). Using the third and fourth order trigonometric identities (A 7–A 15), we can calculate these coefficients

for wave numbers $k \neq n/2$, $k \neq n/3$, and $k \neq n/4$ in the form

$$
\begin{aligned}
&f_{jk}^{(1)} = f_{jk}^{(2)} = 0\,, \quad \text{for} \quad j+k=2\,,\\
&f_{30}^{(1)} = f_{12}^{(1)} = f_{21}^{(2)} = f_{03}^{(2)} = \mathcal{E}\tfrac{3\alpha b_{3\mathrm{cr}}}{4(b_{1\mathrm{cr}})^3}\tfrac{\alpha}{\omega}\big(1+\tfrac{\omega^2}{\alpha^2}\big)\big(\omega+\tfrac{\omega}{\alpha}+\tfrac{\omega^3}{\alpha^2}\big)\,,\\
&f_{21}^{(1)} = f_{03}^{(1)} = -f_{30}^{(2)} = -f_{12}^{(2)} = \mathcal{E}\tfrac{3\alpha b_{3\mathrm{cr}}}{4(b_{1\mathrm{cr}})^3}\tfrac{\alpha}{\omega}\big(1+\tfrac{\omega^2}{\alpha^2}\big)\big(1+2\tfrac{\omega^2}{\alpha^2}\big)\,,\\
&F_{10}^{(1)} = \mathcal{E}\tfrac{2b_{2\mathrm{cr}}}{n(b_{1\mathrm{cr}})^2}\begin{bmatrix}\big(3+\alpha-\tfrac{\omega^2}{\alpha}\big)\widetilde{C}+\big(\tfrac{\alpha}{\omega}-2\omega-2\tfrac{\omega}{\alpha}\big)\widetilde{S}+\big(1+\alpha+\tfrac{\omega^2}{\alpha}\big)E\\ 0\end{bmatrix},\\
&F_{01}^{(1)} = \mathcal{E}\tfrac{2b_{2\mathrm{cr}}}{n(b_{1\mathrm{cr}})^2}\begin{bmatrix}-\big(\tfrac{\alpha}{\omega}-2\omega-2\tfrac{\omega}{\alpha}\big)\widetilde{C}+\big(3+\alpha-\tfrac{\omega^2}{\alpha}\big)\widetilde{S}+\big(\tfrac{\alpha}{\omega}+2\tfrac{\omega}{\alpha}\big)E\\ 0\end{bmatrix},\\
&F_{10}^{(2)} = \mathcal{E}\tfrac{2b_{2\mathrm{cr}}}{n(b_{1\mathrm{cr}})^2}\begin{bmatrix}-\big(\tfrac{\alpha}{\omega}-2\omega-2\tfrac{\omega}{\alpha}\big)\widetilde{C}+\big(3+\alpha-\tfrac{\omega^2}{\alpha}\big)\widetilde{S}-\big(\tfrac{\alpha}{\omega}+2\tfrac{\omega}{\alpha}\big)E\\ 0\end{bmatrix},\\
&F_{01}^{(2)} = \mathcal{E}\tfrac{2b_{2\mathrm{cr}}}{n(b_{1\mathrm{cr}})^2}\begin{bmatrix}-\big(3+\alpha-\tfrac{\omega^2}{\alpha}\big)\widetilde{C}-\big(\tfrac{\alpha}{\omega}-2\omega-2\tfrac{\omega}{\alpha}\big)\widetilde{S}+\big(1+\alpha+\tfrac{\omega^2}{\alpha}\big)E\\ 0\end{bmatrix},\\
&F_{jk}^{(3\mathrm{c})} = F_{jk}^{(3\mathrm{s})} = 0\,,\\
&F_{20}^{(3-)} = F_{02}^{(3-)} = -\tfrac{b_{2\mathrm{cr}}}{(b_{1\mathrm{cr}})^2}\big(1+\tfrac{\omega^2}{\alpha^2}\big)\begin{bmatrix}0\\ E\end{bmatrix},\\
&F_{11}^{(3-)} = 0\,,\\
&F_{20}^{(3)} = \tfrac{b_{2\mathrm{cr}}}{(b_{1\mathrm{cr}})^2}\begin{bmatrix}\big(1-\tfrac{\omega^2}{\alpha^2}\big)\widetilde{C}-2\tfrac{\omega}{\alpha}\widetilde{S}+\big(1+\tfrac{\omega^2}{\alpha^2}\big)E\\ 0\end{bmatrix},\\
&F_{11}^{(3)} = \tfrac{2b_{2\mathrm{cr}}}{(b_{1\mathrm{cr}})^2}\begin{bmatrix}2\tfrac{\omega}{\alpha}\widetilde{C}+\big(1-\tfrac{\omega^2}{\alpha^2}\big)\widetilde{S}\\ 0\end{bmatrix},\\
&F_{20}^{(3)} = \tfrac{b_{2\mathrm{cr}}}{(b_{1\mathrm{cr}})^2}\begin{bmatrix}-\big(1-\tfrac{\omega^2}{\alpha^2}\big)\widetilde{C}+2\tfrac{\omega}{\alpha}\widetilde{S}+\big(1+\tfrac{\omega^2}{\alpha^2}\big)E\\ 0\end{bmatrix},
\end{aligned}
\tag{5.6}
$$

where we use the vectors $\widetilde{C}, \widetilde{S} \in \mathbb{R}^n$ defined by

$$
\widetilde{C} = \begin{bmatrix}\cos(\frac{4k\pi}{n}1)\\ \cos(\frac{4k\pi}{n}2)\\ \vdots\\ \cos(\frac{4k\pi}{n}n)\end{bmatrix}, \quad \widetilde{S} = \begin{bmatrix}\sin(\frac{4k\pi}{n}1)\\ \sin(\frac{4k\pi}{n}2)\\ \vdots\\ \sin(\frac{4k\pi}{n}n)\end{bmatrix}. \tag{5.7}
$$

Note that the cases $k = n/2$, $k = n/3$, and $k = n/4$ result in different formulae for the above coefficients, but the final Poincaré-Lyapunov constant will have the same formula as in the case of general wave number k. The detailed calculation of these 'resonant' cases is not presented here.

Now let us approximate the center-manifold locally as a truncated power series of w depending on the coordinates z_1 and z_2 as

$$
w(\vartheta) = \frac{1}{2}\left(h_{20}(\vartheta)z_1^2 + 2h_{11}(\vartheta)z_1z_2 + h_{02}(\vartheta)z_2^2\right). \tag{5.8}
$$

There are no linear terms since the plane spanned by the eigenvectors s_1 and s_2 is tangent to the center-manifold at the origin. Third and higher order terms are

dropped. The unknown coefficients h_{20}, h_{11} and $h_{02} \in \mathbb{X}_{\mathbb{R}^{2n}}$ can be determined by calculating the derivative of w and substituting that into the third equation of (5.5). The solution of the resulting linear boundary value problem given in details in (Orosz & Stépán 2004) is

$$\begin{aligned}\begin{bmatrix} h_{20}(\vartheta) \\ h_{11}(\vartheta) \\ h_{02}(\vartheta) \end{bmatrix} &= \begin{bmatrix} H_1 \\ H_2 \\ -H_1 \end{bmatrix} \cos(2\omega\vartheta) + \begin{bmatrix} -H_2 \\ H_1 \\ H_2 \end{bmatrix} \sin(2\omega\vartheta) + \begin{bmatrix} H_0 \\ 0 \\ H_0 \end{bmatrix} \\ &- \frac{1}{4\omega} \begin{bmatrix} 0 \\ F_{20}^{(3-)} - F_{02}^{(3-)} \\ 2F_{11}^{(3-)} \end{bmatrix} - \frac{1}{2} \begin{bmatrix} F_{20}^{(3-)} + F_{02}^{(3-)} \\ 0 \\ F_{20}^{(3-)} + F_{02}^{(3-)} \end{bmatrix} \vartheta \,, \end{aligned} \tag{5.9}$$

where the vectors H_0, H_1, and $H_2 \in \mathbb{R}^{2n}$ satisfy

$$\begin{aligned} &\begin{bmatrix} \mathrm{L}+\mathrm{R} & 0 & 0 \\ 0 & \mathrm{L}+\mathrm{R}\cos(2\omega) & 2\omega\mathrm{I}+\mathrm{R}\sin(2\omega) \\ 0 & -\big(2\omega\mathrm{I}+\mathrm{R}\sin(2\omega)\big) & \mathrm{L}+\mathrm{R}\cos(2\omega) \end{bmatrix} \begin{bmatrix} H_0 \\ H_1 \\ H_2 \end{bmatrix} \\ &= -\frac{1}{2} \begin{bmatrix} F_{20}^{(3)} + F_{02}^{(3)} + F_{20}^{(3-)} + F_{02}^{(3-)} \\ F_{20}^{(3)} - F_{02}^{(3)} \\ F_{11}^{(3)} \end{bmatrix} . \end{aligned} \tag{5.10}$$

Here we also used that $F_{jk}^{(3\mathrm{c})} = F_{jk}^{(3\mathrm{s})} = 0$ and

$$\mathrm{R}\big(F_{20}^{(3-)} + F_{02}^{(3-)}\big) = 0 \,, \quad (\mathrm{L}+\mathrm{R})F_{11}^{(3-)} = 0 \,, \quad (\mathrm{L}+\mathrm{R})\big(F_{20}^{(3-)} - F_{02}^{(3-)}\big) = 0 \,, \tag{5.11}$$

in accordance with (5.6).

One can find that the $2n$-dimensional equation for H_0 is decoupled from the $4n$-dimensional equation for H_1, H_2 in (5.10). Since $(\mathrm{L}+\mathrm{R})$ is singular due to the translational symmetry (4.5), the nonhomogeneous equation for H_0 in (5.10) may seem not to be solvable. However, its right-hand side belongs to the image space of the coefficient matrix $(\mathrm{L}+\mathrm{R})$ due to the translational symmetry induced terms $F_{jk}^{(3-)}$. We obtain the solution

$$H_0 = \tfrac{b_{2\mathrm{cr}}}{(b_{1\mathrm{cr}})^2}\big(1 + \tfrac{\omega^2}{\alpha^2}\big) \begin{bmatrix} E \\ \kappa E \end{bmatrix} , \tag{5.12}$$

with the undetermined parameter κ.

At the same time, the nonhomogeneous equation for H_1, H_2 in (5.10) is not effected by the vectors $F_{jk}^{(3-)}$. Using (3.17) this $4n$-dimensional equation leads to

$$\left.\begin{aligned} H_{1,i} &= -2\omega H_{2,n+i} \\ H_{2,i} &= 2\omega H_{1,n+i} \end{aligned}\right\} \quad \text{for} \quad i = 1, \ldots, n \,, \tag{5.13}$$

and to the $2n$-dimensional equation

$$\begin{bmatrix} \mu\sin^2(\frac{k\pi}{n})\,\mathrm{I} - \cos(\frac{2k\pi}{n})\mathrm{A} & \eta\sin^2(\frac{k\pi}{n})\,\mathrm{I} - \sin(\frac{2k\pi}{n})\mathrm{A} \\ -\big(\eta\sin^2(\frac{k\pi}{n})\,\mathrm{I} - \sin(\frac{2k\pi}{n})\mathrm{A}\big) & \mu\sin^2(\frac{k\pi}{n})\,\mathrm{I} - \cos(\frac{2k\pi}{n})\mathrm{A} \end{bmatrix} H_{\cup} = -\tfrac{4b_{2\mathrm{cr}}}{\omega^2 b_{1\mathrm{cr}}}\sin^2(\tfrac{k\pi}{n}) \begin{bmatrix} \widetilde{C} \\ \widetilde{S} \end{bmatrix} , \tag{5.14}$$

where the vector $H_\cup \in \mathbb{R}^{2n}$ is defined as

$$\left.\begin{aligned} H_{\cup,i} &= H_{1,n+i} \\ H_{\cup,n+i} &= H_{2,n+i} \end{aligned}\right\} \quad \text{for} \quad i = 1,\dots,n\,, \tag{5.15}$$

and

$$\mu = \frac{-\frac{16 b_{1\mathrm{cr}}}{\alpha}\frac{\omega^2}{\alpha^2}}{\left(1+\frac{\omega^2}{\alpha^2}\right)^2}\,, \quad \eta = \frac{\frac{8 b_{1\mathrm{cr}}}{\omega}\left(1+3\frac{\omega^2}{\alpha^2}\right)}{\left(1+\frac{\omega^2}{\alpha^2}\right)^2}\,. \tag{5.16}$$

The solution of (5.14) is given by

$$H_\cup = \frac{-\frac{4 b_{2\mathrm{cr}}}{\omega^2 b_{1\mathrm{cr}}}}{\left(\eta - 4\cot(\frac{k\pi}{n})\right)^2+\mu^2}\left(\mu\begin{bmatrix}\widetilde{C}\\ \widetilde{S}\end{bmatrix} + \left(\eta - 4\cot(\tfrac{k\pi}{n})\right)\begin{bmatrix}-\widetilde{S}\\ \widetilde{C}\end{bmatrix}\right)\,, \tag{5.17}$$

which provides

$$\begin{aligned} H_1 &= \frac{\frac{4 b_{2\mathrm{cr}}}{\omega^2 b_{1\mathrm{cr}}}}{\left(\eta - 4\cot(\frac{k\pi}{n})\right)^2+\mu^2}\left(\left(\eta - 4\cot(\tfrac{k\pi}{n})\right)\begin{bmatrix}2\omega\widetilde{C}\\ \widetilde{S}\end{bmatrix} + \mu\begin{bmatrix}2\omega\widetilde{S}\\ -\widetilde{C}\end{bmatrix}\right)\,, \\ H_2 &= \frac{\frac{4 b_{2\mathrm{cr}}}{\omega^2 b_{1\mathrm{cr}}}}{\left(\eta - 4\cot(\frac{k\pi}{n})\right)^2+\mu^2}\left(\left(\eta - 4\cot(\tfrac{k\pi}{n})\right)\begin{bmatrix}2\omega\widetilde{S}\\ -\widetilde{C}\end{bmatrix} - \mu\begin{bmatrix}2\omega\widetilde{C}\\ \widetilde{S}\end{bmatrix}\right)\,. \end{aligned} \tag{5.18}$$

Now, using these in (5.8,5.9) we can calculate $\mathrm{R}w(-1)$ which appears in the first two equations of (5.5). In this way we obtain the flow restricted onto the two-dimensional center-manifold described by the ODEs

$$\begin{bmatrix}\dot z_1\\ \dot z_2\end{bmatrix} = \begin{bmatrix}0 & \omega\\ -\omega & 0\end{bmatrix}\begin{bmatrix}z_1\\ z_2\end{bmatrix} + \begin{bmatrix}\sum_{j,k\geq 0}^{j+k=2,3} f_{jk}^{(1)} z_1^j z_2^k\\ \sum_{j,k\geq 0}^{j+k=2,3} f_{jk}^{(2)} z_1^j z_2^k\end{bmatrix} + \begin{bmatrix}\sum_{j,k\geq 0}^{j+k=3} g_{jk}^{(1)} z_1^j z_2^k\\ \sum_{j,k\geq 0}^{j+k=3} g_{jk}^{(2)} z_1^j z_2^k\end{bmatrix}\,, \tag{5.19}$$

where the coefficients $f_{jk}^{(1,2)}$ have already been determined by (5.6) in (5.5), while the coefficients

$$\begin{aligned} g_{30}^{(1)} &= g_{12}^{(1)} = g_{21}^{(2)} = g_{03}^{(2)} \\ &= \frac{\mathcal{E}\frac{2\alpha(b_{2\mathrm{cr}})^2}{(b_{1\mathrm{cr}})^4}\cot(\frac{k\pi}{n})}{\left(\eta - 4\cot(\frac{k\pi}{n})\right)^2+\mu^2}\frac{\alpha}{\omega}\left(1+\tfrac{\omega^2}{\alpha^2}\right)\left(\left(\eta - 4\cot(\tfrac{k\pi}{n})\right)\left(\omega+\tfrac{\omega}{\alpha}+\tfrac{\omega^3}{\alpha^2}\right) + \mu\left(1+2\tfrac{\omega^2}{\alpha^2}\right)\right)\,, \\ g_{21}^{(1)} &= g_{03}^{(1)} = -g_{30}^{(2)} = -g_{12}^{(2)} \\ &= \frac{\mathcal{E}\frac{2\alpha(b_{2\mathrm{cr}})^2}{(b_{1\mathrm{cr}})^4}\cot(\frac{k\pi}{n})}{\left(\eta - 4\cot(\frac{k\pi}{n})\right)^2+\mu^2}\frac{\alpha}{\omega}\left(1+\tfrac{\omega^2}{\alpha^2}\right)\left(\left(\eta - 4\cot(\tfrac{k\pi}{n})\right)\left(1+2\tfrac{\omega^2}{\alpha^2}\right) - \mu\left(\omega+\tfrac{\omega}{\alpha}+\tfrac{\omega^3}{\alpha^2}\right)\right)\,, \end{aligned} \tag{5.20}$$

originate in the terms involving $\mathrm{R}w(-1)$. To determine (5.20) the trigonometric identities (A 4–A 15) has been used.

We note that the coefficients $f_{jk}^{(1,2)}$ $(j+k=2)$ of the second-order terms are not changed by the center-manifold reduction. The so-called Poincaré-Lyapunov

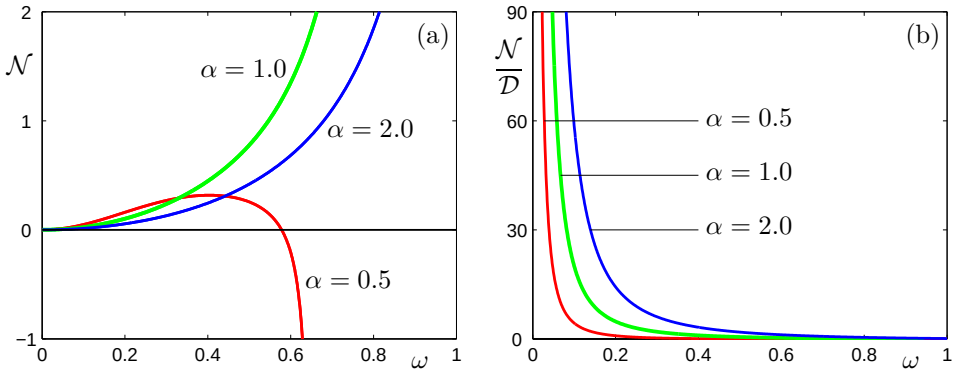

Figure 3. Quantities defined by (5.22,5.23) as a function of the frequency ω, for representative values of parameter α. In panel (a) the numerator $\mathcal{N}(\omega,\alpha)$ is depicted, while panel (b) shows the ratio $\mathcal{N}(\omega,\alpha)/\mathcal{D}(\omega,\alpha)$.

constant in the Poincaré normal form of (5.19) can be determined by the Bautin formula (Stépán 1989)

$$\begin{aligned}\Delta &= \frac{1}{8}\Bigg(\frac{1}{\omega}\Big((f_{20}^{(1)}+f_{02}^{(1)})(-f_{11}^{(1)}+f_{20}^{(2)}-f_{02}^{(2)})+(f_{20}^{(2)}+f_{02}^{(2)})(f_{20}^{(1)}-f_{02}^{(1)}+f_{11}^{(2)})\Big)\\ &\qquad +\Big(3f_{30}^{(1)}+f_{12}^{(1)}+f_{21}^{(2)}+3f_{03}^{(2)}\Big)+\Big(3g_{30}^{(1)}+g_{12}^{(1)}+g_{21}^{(2)}+3g_{03}^{(2)}\Big)\Bigg)\\ &= \mathcal{E}\tfrac{\alpha}{4(b_{1\mathrm{cr}})^3}\tfrac{\alpha}{\omega}\big(1+\tfrac{\omega^2}{\alpha^2}\big)\big(\omega+\tfrac{\omega}{\alpha}+\tfrac{\omega^3}{\alpha^2}\big)\times\\ &\times\frac{1}{2}\left(6b_{3\mathrm{cr}}+\frac{(2b_{2\mathrm{cr}})^2}{b_{1\mathrm{cr}}}\frac{4\cot(\frac{k\pi}{n})}{\big(\eta-4\cot(\frac{k\pi}{n})\big)^2+\mu^2}\left(\eta-4\cot(\tfrac{k\pi}{n})+\mu\frac{1+2\frac{\omega^2}{\alpha^2}}{\omega+\frac{\omega}{\alpha}+\frac{\omega^3}{\alpha^2}}\right)\right).\end{aligned} \tag{5.21}$$

The bifurcation is supercritical for negative and subcritical for positive values of Δ. We found that $\Delta>0$ is always true when $\frac{k}{n}\ll 1$ which is the case for real traffic situations (many vehicles n with a few waves k). This can be proven as is detailed below.

The first part of the expression (5.21) of Δ in front of the parenthesis is always positive since $\mathcal{E},b_{1\mathrm{cr}},\alpha,\omega>0$. Within the parenthesis in (5.21), the first term is positive since (3.16) implies $b_{1\mathrm{cr}}=\mathrm{V}'(h_{\mathrm{cr}}^*)<1/2$, which yields critical headway values h_{cr}^* such that $6b_{3\mathrm{cr}}=\mathrm{V}'''(h_{\mathrm{cr}}^*)>0$ (see Fig. 2(b,d)). The second term in the parenthesis in (5.21) contains the ratio of two complicated expressions, which, by using (3.16,5.16), can be rearranged in the form

$$\begin{aligned}&4\cot(\tfrac{k\pi}{n})\left(\eta-4\cot(\tfrac{k\pi}{n})+\mu\frac{1+2\frac{\omega^2}{\alpha^2}}{\omega+\frac{\omega}{\alpha}+\frac{\omega^3}{\alpha^2}}\right)\\ &=\big(4\cot(\tfrac{k\pi}{n})\big)^2\left(\frac{\big(1+\frac{\omega^2}{\alpha^2}\big)\big(\omega+\frac{\omega}{\alpha}+3\frac{\omega^3}{\alpha^2}\big)-4\frac{\omega^5}{\alpha^5}}{\big(\cos\omega-\frac{\omega}{\alpha}\sin\omega\big)\big(1+\frac{\omega^2}{\alpha^2}\big)\big(\omega+\frac{\omega}{\alpha}+\frac{\omega^3}{\alpha^2}\big)}-1\right)\\ &:=\big(4\cot(\tfrac{k\pi}{n})\big)^2\mathcal{N}(\omega,\alpha)\,,\end{aligned} \tag{5.22}$$

and

$$\begin{aligned}
&\big(\eta - 4\cot(\tfrac{k\pi}{n})\big)^2 + \mu^2 \\
&= \big(4\cot(\tfrac{k\pi}{n})\big)^2 \left(\frac{\big(1+\frac{\omega^2}{\alpha^2}\big)\big(1+4\frac{\omega^2}{\alpha^2}\big) - 2\big(\cos\omega - \frac{\omega}{\alpha}\sin\omega\big)\big(1+3\frac{\omega^2}{\alpha^2}\big)}{\big(\cos\omega - \frac{\omega}{\alpha}\sin\omega\big)^2\big(1+\frac{\omega^2}{\alpha^2}\big)} + 1 \right) \qquad (5.23) \\
&:= \big(4\cot(\tfrac{k\pi}{n})\big)^2 \mathcal{D}(\omega,\alpha) > 0\,.
\end{aligned}$$

Since (5.23) is always positive, the sign of (5.22) is crucial for deciding the overall sign of Δ. According to (3.16) $\omega \in (0, \frac{k\pi}{n})$, that is, the realistic case $\frac{k}{n} \ll 1$ implies the oscillation frequency $\omega \ll 1$.

Fig. 3(a) shows the numerator $\mathcal{N}(\omega,\alpha)$ for some particular values of α demonstrating that $\mathcal{N}(\omega,\alpha) > 0$ for $\omega \ll 1$. Note that if $\alpha \to 0$ then $\mathcal{N}(\omega,\alpha)$ may become negative (see Fig. 3(a) for $\alpha = 0.5$), but this is a physically unrealistic case where drivers intend to reach their desired speed v^0 extremely slowly.

Moreover, the ratio of (5.22) and (5.23), $\mathcal{N}(\omega,\alpha)/\mathcal{D}(\omega,\alpha)$, is not only positive for $\omega \ll 1$ but also $\mathcal{N}(\omega,\alpha)/\mathcal{D}(\omega,\alpha) \to \infty$ when $\omega \to 0$ (i.e., when $n \to \infty$) as shown in Fig. 3(b). This feature provides robustness for subcriticality. Note that subcriticality also occurs for optimal velocity functions different from (2.2), e.g., for those that are considered in (Orosz *et al.* 2004*a*).

Using definition (3.6), formulas (3.18,3.22), and expressions (5.21–5.23), the amplitude A of the unstable oscillations is obtained in the form

$$A = \sqrt{-\frac{\mathrm{Re}\,\big(\lambda_1'(h^*_{\mathrm{cr}})\big)}{\Delta}(h^* - h^*_{\mathrm{cr}})} = \frac{\omega}{\sin(\frac{k\pi}{n})} \sqrt{-2\frac{\mathrm{V}''(h^*_{\mathrm{cr}})\,(h^* - h^*_{\mathrm{cr}})}{\mathrm{V}'''(h^*_{\mathrm{cr}}) + \frac{\big(\mathrm{V}''(h^*_{\mathrm{cr}})\big)^2}{\mathrm{V}'(h^*_{\mathrm{cr}})}\frac{\mathcal{N}(\omega,\alpha)}{\mathcal{D}(\omega,\alpha)}}}\,. \qquad (5.24)$$

Thus, the first Fourier term of the oscillation restricted onto the center-manifold is

$$\begin{bmatrix} z_1(t) \\ z_2(t) \end{bmatrix} = A \begin{bmatrix} \cos(\omega t) \\ -\sin(\omega t) \end{bmatrix}\,. \qquad (5.25)$$

Since close to the critical bifurcation parameter h^*_{cr} we have $y_t(\vartheta) \approx z_1(t)s_1(\vartheta) + z_2(t)s_2(\vartheta)$, equation (5.25) yields

$$\begin{aligned}
y(t) = y_t(0) &\approx z_1(t)s_1(0) + z_2(t)s_2(0) \\
&= A\big(s_1(0)\cos(\omega t) - s_2(0)\sin(\omega t)\big) \qquad (5.26) \\
&= A\big(S_1\cos(\omega t) - S_2\sin(\omega t)\big)\,,
\end{aligned}$$

where the vectors S_1, S_2 are given in (4.31).

Note that zero reaction time delay results in $\mathcal{N}(\omega,\alpha)/\mathcal{D}(\omega,\alpha) \equiv -1$ as shown in (Gasser *et al.* 2004). In that case subcriticality appears only for extremely high values of the desired speed v^0 when the term $6b_{3\mathrm{cr}}$ becomes greater than $(2b_{2\mathrm{cr}})^2/b_{1\mathrm{cr}}$ at the critical points (of the non-delayed model). Consequently, the presence of the drivers' reaction-time delay has an essential role in the robustness of the subcritical nature of the Hopf bifurcation. This subcriticalty explains how traffic waves can be formed when the uniform flow equilibrium is stable, as is detailed in the subsequent section.

6. Physical Interpretation of Results

The unstable periodic motion given in (5.26) corresponds to a spatial wave formation in the traffic flow, which is actually unstable. Substituting (4.31) into (5.26) and using definition (3.7), one can determine the velocity perturbation of the ith car as

$$\dot{x}_i^{\mathrm{p}}(t) = A\cos\big(\tfrac{2\pi k}{n} i + \omega t\big)\,. \tag{6.1}$$

The interpretation of this perturbation mode is a wave travelling opposite to the car flow with spatial wave number k (i.e., with spatial wavelength $L/k = h^* n/k$). The related wave speed is

$$c_{\mathrm{wave}}^{\mathrm{p}} = -\tfrac{n}{2k\pi} h^* \omega < 0\,, \tag{6.2}$$

where the elimination of the frequency ω with the help of (3.18) leads to

$$c_{\mathrm{wave}}^{\mathrm{p}} = -h^* b_{1\mathrm{cr}} \Big(1 - \mathcal{O}\big(\tfrac{k\pi}{n}\big)^2\Big)\,. \tag{6.3}$$

Since the uniform flow equilibrium (3.1) travels with speed $v^* = \mathrm{V}(h^*)$, the speed of the arising wave is

$$c_{\mathrm{wave}} = v^* + c_{\mathrm{wave}}^{\mathrm{p}} = \mathrm{V}(h^*) - h^* \mathrm{V}'(h_{\mathrm{cr}}^*) \Big(1 - \mathcal{O}\big(\tfrac{k\pi}{n}\big)^2\Big)\,. \tag{6.4}$$

By considering the optimal velocity function (2.2), we obtain $c_{\mathrm{wave}} < 0$, that is, the resulting wave propagates in the opposite direction to the flow of vehicles. Note that the non-delayed model introduced in (Bando *et al.* 1995) exhibits the same wave speed apart from some differences in the coefficient of the correction term $\mathcal{O}\big(\tfrac{k\pi}{n}\big)^2$. If one neglects this correction term, the wave speed becomes independent of n and k, which corresponds to the results obtained from continuum models; see e.g., (Whitman 1999).

In order to check the reliability of the Poincaré-Lyapunov constant (5.21) and the amplitude estimation (5.24), we compare these analytical results with those obtained by numerical continuation techniques with the package DDE-BIFTOOL (Engelborghs *et al.* 2001). In Fig. 4 we demonstrate the subcriticality for $n = 9$ cars and $k = 1$ wave. The horizontal axis corresponds to the uniform flow equilibrium, that is, stable for small and large values of h^* (shown by green solid line) but unstable for intermediate values of h^* (shown by red dashed line) in accordance with formula (3.16) and Fig. 2(b). The Hopf bifurcations, where the equilibrium loses its stability, are marked by blue stars. The branches of the arising unstable periodic motions given by (5.24) are shown as red dashed curves.

According to numerical simulations and traffic experiments, a stable oscillating state is expected 'outside' the unstable oscillating state. This includes travelling with the desired speed v^0, decelerating, stopping, and accelerating. In Fig. 4 the horizontal green line at $A = v^0/2$ represents these stable *stop-and-go oscillations*. The corresponding *stop-and-go wave* propagates against the traffic flow. Vehicles leave the traffic jam at the front and enter it at the back (see Fig. 1). The above analytic construction reveals wide regions of bistability on both sides of the unstable equilibrium. In such domains, depending on the initial condition, the system either tends to the uniform flow equilibrium or to the stop-and-go wave.

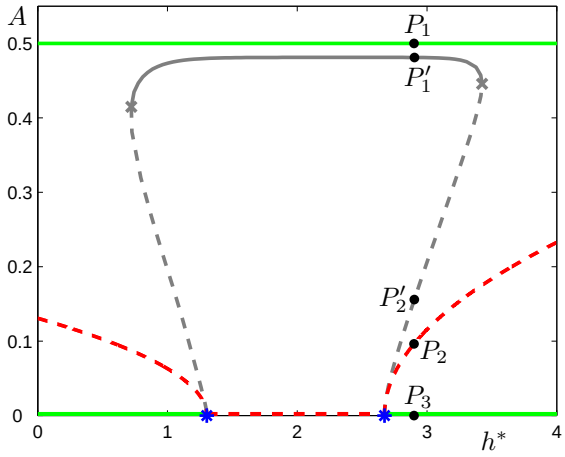

Figure 4. The amplitude A of velocity oscillations as a function of the average headway parameter h^* for $n = 9$ cars, $k = 1$ wave, and parameters $\alpha = 1.0$, $v^0 = 1.0$. The horizontal axis ($A \equiv 0$) represents the uniform flow equilibrium. The analytical results are coloured: green solid and red dashed curves represent stable and unstable branches, respectively, and blue stars stand for Hopf bifurcations. Grey curves correspond to numerical continuation results: solid and dashed curves refer to stable and unstable states, and grey crosses represent fold bifurcations. The points marked by P_i, P_i' refer to the oscillation profiles presented in Fig. 5.

In Fig. 4, we also displayed the results of numerical continuation carried out with the package DDE-BIFTOOL (Engelborghs *et al.* 2001). Grey solid curves represent stable oscillations while grey dashed curves represent unstable ones. The fold bifurcation points, where the branches of stable and unstable oscillations meet, are marked by grey crosses. The comparison of the results shows that the analytical approximation of the unstable oscillations is quantitatively reliable in the vicinity of the Hopf bifurcation points. The analytical amplitude $v^0/2$ of the stop-and-go oscillations is slightly larger than the numerically computed ones. The analytically suggested bistable region is larger than the computed one, since the third degree approximation is not able to predict fold bifurcations of periodic solutions (the grey crosses in Fig. 4). In order to find these fold bifurcation points it is necessary to use numerical continuation techniques as presented in (Orosz *et al.* 2004*b*). Nevertheless, qualitatively the same structure is obtained by the two different techniques.

As was already mentioned in Section 3, the wave numbers $k > 1$ are related to Hopf bifurcations in the parameter region where the uniform flow equilibrium is already unstable. This also means that the corresponding oscillations for $k > 1$ are unstable independently of the criticality of these Hopf bifurcations. Still, we found that these Hopf bifurcations are all robustly subcritical for any wave number k (except for large $\frac{k}{n} \simeq 1/2$). Consequently, the only stable oscillating state is the stop-and-go motion for $k = 1$. On the other hand, several unstable solutions may coexist as is explained in (Orosz *et al.* 2004*b*). Note that analytical and numerical results agree better as the wave number k is increased because the oscillating solution becomes more harmonic.

To represent the features of vehicles' motions, the velocity oscillation profiles

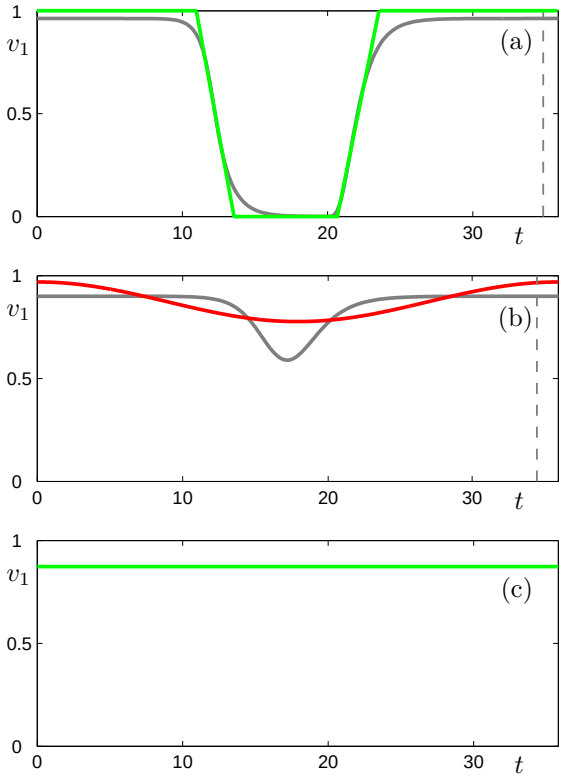

Figure 5. Velocity profiles of the first car for the points marked in Fig. 4. Colored curves are calculated analytically while grey curves are computed by numerical continuation. In panel (a) the stable stop-and-go oscillations are shown for point P_1 in green and for point P_1' in grey, while in panel (b) the unstable oscillations are displayed for point P_2 in red and for point P_2' in grey. In panel (c) the stable uniform flow solution is depicted for point P_3 in green.

of the first vehicle are shown in Fig. 5 for the points P_i, P_i' marked in Fig. 4, for headway $h^* = 2.9$. Again, the colored curves correspond to the analytical results, while the grey curves are obtained by numerical continuation. In Fig. 5, the time window of each panel is chosen to be the period of the first Fourier approximation given by (3.18) (red curve in panel (b)). The dashed vertical lines in panels (a,b) indicate oscillation periods computed numerically with DDE-BIFTOOL.

Panel (a) of Fig. 5 shows the stop-and-go oscillations. The analytical construction (green curve) is obtained by assuming that the stopping and flowing states are connected with states of constant acceleration/deceleration, which is qualitatively a good approximation of the numerical result (grey curve). Panel (b) compares the unstable periodic motions computed analytically (red curve) from the Hopf calculation with those from numerical continuation (grey curve). These exist around the stable uniform flow equilibrium shown in panel (c).

For a perturbation 'smaller' than the unstable oscillation, the system approaches the uniform flow equilibrium. If a larger perturbation is applied then the system

develops stop-and-go oscillations and a spatial stop-and-go travelling wave appears as demonstrated in Fig. 1. Since the period of the stable and unstable oscillations are close to each other, the stable stop-and-go wave travels approximately with the speed of the unstable travelling wave (see (6.4) for $k = 1$).

7. Conclusion

A non-linear car-following model has been investigated with special attention paid to the reaction-time delay of drivers. By considering the average headway as a bifurcation parameter, Hopf bifurcations were identified. In order to investigate the resulting periodic motions, the singularities related to the essential translational symmetry had to be eliminated. Then the Hopf bifurcations were found to be robustly subcritical leading to bistability between the uniform flow equilibrium and a stop-and-go wave. The appearing oscillations manifest themselves as spatial waves propagating backward along the circular road.

In the non-delayed model of (Bando *et al.* 1995) subcriticality and bistablity occur only for extremely high values of the desired speed v^0, as it is demonstrated in (Gasser *et al.* 2004). We proved that subcriticality and bistablity are robust features of the system due to the drivers' reaction-time delay, even for moderate values of the desired speed. This delay, which is smaller than the macroscopic time-scales of traffic flow, plays an essential role in this complex system because it changes the qualitative nonlinear dynamics of traffic.

Due to the subcriticality, stop-and-go traffic jams can develop for large enough perturbations even when the desired uniform flow is linearly stable. These perturbations can be caused, for example, by a slower vehicle (such us a lorry) joining the inner lane flow for a short time interval via changing lanes. It is essential to limit these unwanted events, for example, by introducing temporary regulations provided by overhead gantries. Still, if a backward travelling wave shows up without stoppings, it either dies out by itself or gets worse ending up as a persistent stop-and-go travelling wave. In order to dissolve this undesired situation, an appropriate control can be applied using temporary speed limits given by gantries that can lead the traffic back 'inside' the unstable travelling wave and then to reach the desired uniform flow. For example, the MIDAS system (Lunt & Wilson 2003) installed on the M25 motorway around London is able to provide the necessary instructions for drivers.

Acknowledgments: The authors acknowledge with thanks discussions with and comments of Eddie Wilson and Bernd Krauskopf on traffic dynamics and on numerical bifurcation analysis. This research was supported by the University of Bristol under a Postgraduate Research Scholarship and by the Hungarian National Science Foundation under grant no. OTKA T043368.

Appendix A. Appendix - Trigonometrical Identities

Considering the wave numbers $k = 1, \ldots, n/2$ (even n) or $k = 1, \ldots, (n-1)/2$ (odd n)

$$\sum_{i=1}^{n} \exp(\mathrm{i}\varrho\tfrac{2k\pi}{n}i) = \begin{cases} 0\,, & \text{if} \quad k \neq n/\varrho\,, \\ n\,, & \text{if} \quad k = n/\varrho\,, \end{cases} \tag{A 1}$$

where $\mathrm{i}^2 = -1$ and $\rho = 1, \ldots, 4$. Therefore, the following identities can be proven. In first order

$$\sum_{i=1}^{n} \cos(\tfrac{2k\pi}{n}i) = 0\,, \tag{A 2}$$

$$\sum_{i=1}^{n} \sin(\tfrac{2k\pi}{n}i) = 0\,. \tag{A 3}$$

In second order

$$\sum_{i=1}^{n} \cos^2(\tfrac{2k\pi}{n}i) = \begin{cases} n/2\,, & \text{if} \quad k \neq n/2\,, \\ n\,, & \text{if} \quad k = n/2\,, \end{cases} \tag{A 4}$$

$$\sum_{i=1}^{n} \sin^2(\tfrac{2k\pi}{n}i) = \begin{cases} n/2\,, & \text{if} \quad k \neq n/2\,, \\ 0\,, & \text{if} \quad k = n/2\,, \end{cases} \tag{A 5}$$

$$\sum_{i=1}^{n} \cos(\tfrac{2k\pi}{n}i)\sin(\tfrac{2k\pi}{n}i) = 0\,. \tag{A 6}$$

In third order

$$\sum_{i=1}^{n} \cos^3(\tfrac{2k\pi}{n}i) = \begin{cases} 0\,, & \text{if} \quad k \neq n/3\,, \\ n/4\,, & \text{if} \quad k = n/3\,, \end{cases} \tag{A 7}$$

$$\sum_{i=1}^{n} \sin^3(\tfrac{2k\pi}{n}i) = 0\,, \tag{A 8}$$

$$\sum_{i=1}^{n} \cos^2(\tfrac{2k\pi}{n}i)\sin(\tfrac{2k\pi}{n}i) = 0\,, \tag{A 9}$$

$$\sum_{i=1}^{n} \cos(\tfrac{2k\pi}{n}i)\sin^2(\tfrac{2k\pi}{n}i) = \begin{cases} 0\,, & \text{if} \quad k \neq n/3\,, \\ -n/4\,, & \text{if} \quad k = n/3\,. \end{cases} \tag{A 10}$$

In fourth order

$$\sum_{i=1}^{n} \cos^4(\tfrac{2k\pi}{n}i) = \begin{cases} 3n/8\,, & \text{if} \quad k \neq n/2 \quad \text{and} \quad k \neq n/4\,, \\ n\,, & \text{if} \quad k = n/2\,, \\ n/2\,, & \text{if} \quad k = n/4\,, \end{cases} \tag{A 11}$$

$$\sum_{i=1}^{n} \sin^4(\tfrac{2k\pi}{n}i) = \begin{cases} 3n/8\,, & \text{if} \quad k \neq n/2 \quad \text{and} \quad k \neq n/4\,, \\ 0\,, & \text{if} \quad k = n/2\,, \\ n/2\,, & \text{if} \quad k = n/4\,, \end{cases} \tag{A 12}$$

$$\sum_{i=1}^{n} \cos^3(\tfrac{2k\pi}{n} i) \sin(\tfrac{2k\pi}{n} i) = 0\,, \tag{A 13}$$

$$\sum_{i=1}^{n} \cos(\tfrac{2k\pi}{n} i) \sin^3(\tfrac{2k\pi}{n} i) = 0\,, \tag{A 14}$$

$$\sum_{i=1}^{n} \cos^2(\tfrac{2k\pi}{n} i) \sin^2(\tfrac{2k\pi}{n} i) = \begin{cases} n/8\,, & \text{if} \quad k \neq n/2 \quad \text{and} \quad k \neq n/4\,, \\ 0\,, & \text{if} \quad k = n/2\,, \\ 0\,, & \text{if} \quad k = n/4\,. \end{cases} \tag{A 15}$$

References

Bando, M., K. Hasebe, A. Nakayama, A. Shibata and Y. Sugiyama (1995). Dynamical model of traffic congestion and numerical simulation. *Physical Review E* **51**(2), 1035–1042.

Bando, M., K. Hasebe, K. Nakanishi and A. Nakayama (1998). Analysis of optimal velocity model with explicit delay. *Physical Review E* **58**(5), 5429–5435.

Berg, P. and R. E. Wilson (2005). Bifurcation analysis of meta-stability and waves of the OV model. In: *Traffic and Granular Flow '03* (S. P. Hoogendoorn, S. Luding, P. H. L. Bovy, M. Schreckenberg and D. E. Wolf, Eds.). Springer-Verlag, Berlin.

Campbell, S. A. and J. Bélair (1995). Analytical and symbolically-assisted investigations of Hopf bifurcations in delay-differential equations. *Canadian Applied Mathematics Quarterly* **3**(2), 137–154.

Davis, L. C. (2003). Modification of the optimal velocity traffic model to include delay due to driver reaction time. *Physica A* **319**, 557–567.

Diekmann, O., S. A. van Gils, S. M. Verduyn Lunel and H. O. Walther (1995). *Delay Equations: Functional-, Complex-, and Nonlinear Analysis*. Vol. 110 of *Applied Mathematical Sciences*. Springer-Verlag, New York.

Doedel, E. J., A. R. Champneys, T. F. Fairgrieve, Yu. A. Kuznetsov, B. Sandstede and X. Wang (1997). AUTO97: Continuation and bifurcation software for ordinary differential equations. Technical report. Department of Computer Science, Concordia University. `http://indy.cs.concordia.ca/auto/`.

Engelborghs, K., T. Luzyanina and G. Samaey (2001). DDE-BIFTOOL v. 2.00: a Matlab package for bifurcation analysis of delay differential equations. Technical Report TW-330. Department of Computer Science, Katholieke Universiteit Leuven, Belgium. `http://www.cs.kuleuven.ac.be/~koen/delay/ddebiftool.shtml`.

Gasser, I., G. Sirito and B. Werner (2004). Bifurcation analysis of a class of 'car-following' traffic models. *Physica D* **197**(3-4), 222–241.

Guckenheimer, J. and P. Holmes (1997). *Nonlinear Oscillations, Dynamical Systems, and Bifurcations of Vector Fields*. Vol. 42 of *Applied Mathematical Sciences*. 3rd ed.. Springer-Verlag, New York.

Hale, J. K. and S. M. Verduyn Lunel (1993). *Introduction to Functional Differential Equations*. Vol. 99 of *Applied Mathematical Sciences*. Springer-Verlag, New York.

Hale, J. K., L. T. Magelhães and W. M. Oliva (2002). *Dynamics in Infinite Dimensions*. Vol. 47 of *Applied Mathematical Sciences*. 2nd ed.. Springer-Verlag, New York.

Hassard, B. D., N. D. Kazarinoff and Y.-H. Wan (1981). *Theory and Applications of Hopf Bifurcation*. Vol. 41 of *London Mathematical Society Lecture Note Series*. Cambridge University Press, Cambridge.

Kerner, B. S. (1999). The physics of traffic. *Physics World* (August), 25–30.

Kolmanovskii, V. B. and A. D. Myshkis (1999). *Introduction to the Theory and Applications of Functional Differential Equations*. Vol. 463 of *Mathematics and Its Applications*. Kluwer Academic Publishers, London.

Kuznetsov, Yu. A. (1998). *Elements of Applied Bifurcation Theory*. Vol. 112 of *Applied Mathematical Sciences*. 2nd ed.. Springer-Verlag, New York.

Lunt, G. and R. E. Wilson (2003). New data sets and improved models of highway traffic. In: *Proceedings of the 35th UTSG Conference*. University of Loughborough, England.

Orosz, G. (2004). Hopf bifurcation calculations in delayed systems. *Periodica Polytechnica* **48**(2), 189–200.

Orosz, G. and G. Stépán (2004). Hopf bifurcation calculations in delayed systems with translational symmetry. *Journal of Nonlinear Science* **14**(6), 505–528.

Orosz, G., R. E. Wilson and B. Krauskopf (2004*a*). Global bifurcation investigation of an optimal velocity traffic model with driver reaction time. *Physical Review E* **70**(2), 026207.

Orosz, G., B. Krauskopf and R. E. Wilson (2004*b*). Bifurcations and multiple traffic jams in a car-following model with reaction time delay. Bristol Centre for Applied Nonlinear Mathematics Preprint 2004.31, University of Bristol, `http://www.enm.bris.ac.uk/anm/preprints/2004r31.html`.

Rottschäfer, V. and B. Krauskopf (2004). A three-parameter study of external cavity modes in semiconductor lasers with optical feedback. In: *Fifth IFAC Workshop on Time-Delay Systems* (W. Michiels and D. Roose, Eds.). International Federation of Automatic Control (IFAC), Leuven, Belgium.

Stépán, G. (1986). Great delay in a predator-prey model. *Nonlinear Analysis TMA* **10**(9), 913–929.

Stépán, G. (1989). *Retarded Dynamical Systems: Stability and Characteristic Functions*. Vol. 210 of *Pitman Research Notes in Mathematics*. Longman, Essex, England.

Stone, E. and S. A. Campbell (2004). Stability and bifurcation analysis of a nonlinear DDE model for drilling. *Journal of Nonlinear Science* **14**(1), 27–57.

Verduyn Lunel, S. M. and B. Krauskopf (2000). The mathematics of delay equations with an application to the Lang-Kobayashi equations. In: *Fundamental Issues of Nonlinear Laser Dynamics* (B. Krauskopf and D. Lenstra, Eds.). Vol. 548 of *AIP Conference Proceedings*. American Institute of Physics, Melville, New York. pp. 66–86.

Whitman, G. B. (1999). *Linear and Nonlinear Waves*. Wiley-Interscience, New York.